iScience, Volume *23*

Supplemental Information

Retinal Degeneration Caused by Rod-Specific *Dhdds* Ablation Occurs without Concomitant Inhibition of Protein *N*-Glycosylation

Sriganesh Ramachandra Rao, Lara A. Skelton, Fuguo Wu, Agnieszka Onysk, Grzegorz Spolnik, Witold Danikiewicz, Mark C. Butler, Delores A. Stacks, Liliana Surmacz, Xiuqian Mu, Ewa Swiezewska, Steven J. Pittler, and Steven J. Fliesler

SUPPLEMENTAL TABLES

ANTIBODY	***SOURCE/VENDOR***	***IDENTIFIER***
Anti-Opsin	Abcam	ab5417 RRID: AB_304874
Anti-GFAP	Dako Agilent	Z0334 RRID: AB_10013382
Anti-Iba1	Abcam	ab178846 RRID: AB_2636859
Anti-Cone Arrestin	Gift: Dr. Cheryl Craft USC, California, USA	PMID: 18701071
Anti-LAMP2	Abcam	ab13524 RRID: AB_2134736
Anti-GLUL	BD Biosciences	610517 RRID: AB_397879
Anti-ICAM1	R&D Systems	AF796
Anti-ACTB	Cell Signaling Technologies	4970 RRID: AB_2223172
Rabbit IgG	Sigma Aldrich	12-370
Mouse IgG	Sigma Aldrich	12-371
LECTIN	***SOURCE/VENDOR***	***IDENTIFIER***
Biotinylated Concanavalin-A	Vector Laboratories	B-1005 RRID: AB_2336346
AF647-Peanut Agglutinin	Thermo Fisher Scientific	L32460
AF647-Wheat Germ Agglutinin	Thermo Fisher Scientific	W32466
ASSAY	***SOURCE/VENDOR***	***IDENTIFIER***
PNGase-F Assay	New England Biolabs	P0704S
BaseScope ISH Assay	ACD Biotech	323900, 323910
Mouse Cytokine Assay	R&D Biosystems	ARY006
TUNEL Assay	Promega Corp.	G3250

Table S1. **Vendor information and identifiers for key reagents utilized in the study. Related to Figures 1 through 6 and Figures S1 through S13.**

TRANSPARENT METHODS

Materials and reagents

All reagents and materials utilized for SDS-PAGE and Western blot analyses were obtained from Bio-Rad Laboratories (Hercules, CA, USA). Other reagents were obtained from Sigma-Aldrich (St. Louis, MO, USA), unless otherwise stated. Plasticware (Falcon™) and all other general lab supplies were obtained from ThermoFisher Scientific (Waltham, MA, USA), unless otherwise indicated.

Generation of rod photoreceptor-specific DHDDS KO mouse

Two constructs containing lacZ flanked by FLP-FRT and *Dhdds* exon 3 flanked by loxP sites were obtained from the Knockout Mouse Project (Clones EPD0137_7_D05, EPD0137_7_D06; KOMP, UC Davis) and were linearized and introduced into mouse ES cells at the Roswell Park Comprehensive Cancer Center (RPCCC) Gene Targeting and Transgenic Facility (Buffalo, NY, USA) using standard technology. The lacZ cassette was excised from the established ES cells with FLP-FRT recombinase, and excision was confirmed by PCR with primers *Dhdds*-FWD: 5'-GTGTCATCCCCTGCTGCAGAT-3' and *Dhdds*-REV: 5'-TGGGTGTAGTGGCTCAGGTC-3', designed in a region that is conserved in both WT and floxed alleles and in the region around the loxP sites. PCR products amplified are 393 and 517 bp for the WT and floxed alleles, respectively. These primers were used to verify the presence of the *Dhdds*$^{flx/flx}$ alleles in all subsequent breedings. Verified Dhdds$^{flx/+}$ heterozygous mice were crossbred to generate homozygotes. In the Rho-iCre (iCre-75) mouse line, Cre recombinase transgene expression in rod photoreceptors is driven by the opsin (RHO) promoter (Li et al., 2005). *Dhdds*$^{flx/flx}$ mice were crossed with Rho-iCre (iCre-75) mice (Stock 015850, RRID: IMSR_JAX:015850, The Jackson Laboratory, Bar Harbor, MN, USA) to generate first filial generation (F1) rod photoreceptor-specific heterozygous

knockouts (Dhdds$^{flx/+}$ iCre^{+}), which were bred to homozygous *Dhdds*$^{flx/flx}$ mice to generate an F2 *Dhdds* knockout line that is homozygous for *the* floxed allele and heterozygous for iCre (*Dhdds*$^{flx/flx}$ iCre^{+}). PCR verification of Cre transgene modification was carried out using forward and reverse primers, 5'-TCAGTGCCTGGAGTTGCG-CTGTGG-3' and 5'-CTTAAAGGCCAGGGCCTGCTTGGC-3' yielding a 650 bp product. The PCR assay for Cre-recombinase does not differentiate between homozygous and heterozygous transgenic mice. For the PCR assay involving direct tissue genotyoping, primers [FWD: 5'-GTGTCATCCCCTGCT-GCAGAT-3', REV: 5'-GTGAAACAAGAACCATTTACCT-3'] were designed upstream of the upstream loxP site, and downstream of downstream loxP site [**Fig. 2**], predicted to yield a specific 584 bp remnant intronic region (due to exon 3 excision). Primers were designed to amplify an unaltered gene loci (*Dhcr7)* as a positive control using the following primer set: FWD 5' – CCCTAGTCACAACTTATGGCCCTT – 3', and REV 5' – TAGTTCCCACAGGTGACATTA – 3', which generates a 375 bp product

Rod-photoreceptor-specific expression and activity of Cre-recombinase in Rho-iCre75 mice was verified by breeding the mouse line to ZsGreen reporter mouse strain (B6.Cg-Gt(ROSA)26Sortm6(CAG-ZsGreen1)Hze/J, Stock# 007906, RRID: IMSR_JAX:007906; The Jackson Laboratory). The first filial, iCre^{+} progeny of the cross would yield ZsGreen expression exclusively in Cre recombinase-expressing cell types, by deleting the loxP sites flanking the STOP codon upstream of the ZsGreen gene.

Animals were maintained on a 12-h light:12-h dark cyclic light schedule (20-40 lux ambient light intensity at cage level), at 22-25°C, and typically were sacrificed 6 h into the light phase. All procedures conformed to the National Research Council's *Guide for the Care and Use of Laboratory Animals* (https://grants.nih.gov/grants/olaw/Guide-for-the-Care-and-use-of-laboratory-animals.pdf).

PCR and mutation verification

Genomic DNA from mouse tail snips was extracted using a Proteinase K-based method (Malumbres et al., 1997). Briefly, mouse tail snips were incubated for 4 h at 55°C in All^{ele}-In-One™ Mouse Tail Direct PCR buffer (Allele Biotechnology, San Diego, CA, USA; ABP-PP-MT01500). The one-step reaction makes the tail genomic DNA available for PCR amplification without purification. PCR amplification was performed using GreenTaq® DNA Polymerase (Sigma-Aldrich, S4438), and the MyIQ™ Single Color Real-Time PCR Detection System (Bio-Rad Laboratories; 170-9740) with cycles of 95ºC denaturation. Extension period for indirect and direct (tail snip and retina) genotyping was 45s at 54°C. The PCR products obtained using the primers described above were electrophoretically separated in a 1.5% agarose gel and stained with EtBr to verify product size, in comparison with a DNA size standard (ThermoFisher Scientific, 15628019), and visualized using a FOTODYNE FOTO/UV® 21 Transilluminator (FOTODYNE Inc.).

SDS-PAGE, Western blot and densitometric analyses

Retinas from age-matched WT and *Dhdds*$^{flx/flx}$ iCre^{+} mice were harvested, and flash frozen immediately. Retinas were lysed with RIPA buffer (ThermoFisher Scientific, 89900) supplemented with protease inhibitor cocktail (ThermoFisher Scientific, 78441) at 1:100 dilution. Protein yield was estimated using a Pierce™ BCA Protein Assay Kit (ThermoFisher Scientific, 23225). Western blot analysis was performed essentially as described previously (Ramachandra Rao et al., 2018), utilizing the following antibodies: mouse anti-opsin monoclonal antibody (Abcam, Burlingame, CA, USA; ab5417, RRID: AB_304874; 1:2000); rat anti-LAMP2 (Abcam, ab13524, RRID: AB_2134736; 1:1000); mouse anti-GLUL [BD Biosciences, San Jose, CA, USA; 610517, RRID: AB_397879; 1:1000], goat anti-ICAM-1 [R&D Systems, Minneapolis, MN, USA, AF796; 1:1000),

rabbit anti-ACTB (Cell Signaling Technology, Danvers, MA, USA; 4970, RRID: AB_2223172; 1:1000), and rabbit anti-GFAP (Dako Agilent, Sanata Clara, CA, USA; Z0334; 1:1000). Blots were then probed with appropriate host-specific alkaline phosphatase-tagged secondary antibodies (1h at room temperature). Detection of antibody binding was achieved using chemifluorescent enzyme substrate (GE Healthcare Life Sciences, Marlborough, MA, USA; 45000947) and a ChemiDoc™ MP Imaging System (Bio-Rad Laboratories). Semi-quantitative densitometry was performed using BioRad ImageLab® software.

Immunohistochemistry, on-section PNGase-F assay, and confocal microscopy

Eyes from WT and *Dhdds*-knockout animals were enucleated (6 h post light onset), fixed in 4% (w:v) formaldehyde (prepared from paraformaldehyde; Electron Microscopy Sciences, Hatfield, PA, USA; 30525-89-4)) in PBS on ice overnight, and then rinsed in chilled PBS three times. Fixed eyes were paraffin embedded, and 10-µm thick sections were collected onto glass Gold Seal™ UltraFrost™ microscope slides. The sections were de-paraffinized and antigen retrieval was carried out as described previously (Emoto et al., 2005). Immunohistochemistry was performed as described previously (Ramachandra Rao et al., 2018) using the following antibodies: mouse anti-opsin (Abcam, RRID: AB_304874; 1:200); rabbit anti-GFAP (Dako Agilent, Z0334, RRID: AB_10013382, 1:100); anti-Iba-1 (Abcam, ab178846, RRID: AB_2636859; 1:100); rabbit anti-cone arrestin (kind gift by Dr. Cheryl Craft, University of South California, USA). Negative controls consisted of nonimmune IgG (10 µg/ml) (Sigma-Aldrich; rabbit: 12-370, mouse: 12-371): from the same host species as that from which the primary antibody was derived. After three rinses with TBST (Tris-buffered saline, containing 0.2% (v/v) Tween-20), tissue sections were incubated for 45 min at room temperature with secondary IgG from suitable host species, conjugated with Alexa Fluor® 488/568/647 (1:500 in antibody diluent; ThermoFisher).

On-section PNGase-F *N*-glycosidase assay (New England Biolabs Inc., Ipswich, MA, USA; P0704S) was carried out as per manufacturer's instructions. Briefly, each retinal section was treated with 200 U of PNG-ase F in 1X Glycobuffer 2 (10X buffer provided with the kit) supplemented with 1% NP-40 detergent at 37^{O}C, overnight. WT and *Dhdds*$^{flx/flx}$ iCre^{+} retinal sections ± PNGase-F were incubated with biotinylated Concanavalin-A (Vector Laboratories, Burlingame, CA, USA: B-1005, RRID: AB_2336346; 1:100), followed by incubation with AF488-conjugated streptavidin (Thermo Fisher Scientific, S11223) and AF647-conjugated Peanut Agglutinin (Thermo Fisher Scientific, L32460). AF647-conjugated Wheat germ agglutinin (Thermo Fisher Scientific, W32466) was utilized to test the synthesis of glycans containing N-acetyl-D-glucosamine.

Slides were rinsed with TBS, counterstained with DAPI (4',6-diamido-2-phenylindole), coverslip mounted using Vectashield® mounting medium (Vector Laboratories, Burlingame, CA; H-1000), and examined with a Leica TCS SPEII DMI4000 scanning laser confocal fluorescence microscope (Leica Microsystems, Buffalo Grove, IL). Images were captured using a 40X oil immersion (RI-1.518) objective under nominal laser intensity (10% of maximum intensity), gain (850) and offset (-0.5) values, to optimize the signal-to-noise ratio.

In Situ Hybridization (ISH)

For the purpose of morphologic verification of successful deletion of exon 3 of *Dhdds*, we utilized an ISH methodology called BaseScope™ (ACDBio, CA, USA). Two sets of short 50 bp complimentary probes (which bind to the target mRNA, spanning a total of ~100bp), conventionally called "ZZ probes", were custom-designed to detect transcript region corresponding to *Dhdds* exon 3 (bp 361-455 of NM_026144.4). ISH was performed according to manufacturer instruction protocol (ACDBio, 323910 and 323900). High signal/noise ratio enables

visualization of specific stretches of the *Dhdds* target mRNA (in this case, *Dhdds)* as a single red chromogenic dot. Corresponding brightfield images were captures using Nikon 80i Fluorescence Microscope equipped with a digital camera and Image Pro analysis software (Nikon Instruments Inc., New York, USA)

Spectral Doman Optical Coherence Tomography (SD-OCT) analysis

All mice were maintained under a 12:12 light/dark cycle, at 20-40 Lux ambient room illumination. Overall retinal morphology and ONL thickness were periodically monitored and recorded non-invasively in age-matched C57BL/6J control and *Dhdds*$^{flx/flx}$ iCre^{+} mice, using a Bioptigen 840 nm UHR-SD-OCT instrument (Bioptigen, NC, USA) essentially as described previously (Butler and Sullivan, 2018). Mice were anesthetized using ketamine-xylazine (75 mg/kg-5 mg/kg) by intraperitoneal injection. Both pupils were dilated using 1% Atropine (Acorn Inc., NDC 17478-215-05). Following dilation, mice were positioned into the instruments AIM-RAS (animal imaging mount and rodent alignment stage) positioning setup, which allows for proper alignment of the mouse eye with the mouse retina bore. Horizontal SD-OCT scans (1.4 mm) were acquired, and B-scan cross-sectional images were analyzed. The image resolution allowed accurate determination of the integrity of the ONL and other retinal layers. The total ONL thickness was defined as the hyporeflective layer observed between the hyper-reflective OS and hyper-reflective OPL. ONL thickness around the optic nerve head (ONH) was measured in control and *Dhdds*$^{flx/flx}$ iCre^{+} mice, at PN 4, 5 and 6 weeks (n=4/group), utilizing Bioptigen InVivoVue® Clinic software. Layer thicknesses were measured manually. The measured ONL thickness was plotted as a function of distance from the ONH, and for statistical analysis one-way ANOVA was performed within GraphPad Prism® software (GraphPad Software, San Diego, CA, USA; RRID: SCR_002798).

Electron microscopy

Mouse eyes were processed for plastic embedment ultramicrotomy, and EM analysis as described in detail previously (Fliesler et al., 2004). In brief, a slit was made in the superior cornea with a razor blade and the eyes were fixed overnight at 4°C in fresh Karnovsky's fixative (0.125 M sodium cacodylate buffer (pH 7.4), containing 2.5% (v/v) glutaraldehyde, 2.0% formaldehyde and 0.025% $CaCl_2$). The fixed eyes were then rinsed with 0.1 M sodium cacodylate buffer (pH 7.4) containing 0.025% $CaCl_2$, and post-fixed for 1 h in 1% (w/v) osmium tetroxide in 0.1 M sodium cacodylate buffer. After post-fixation, the eyes were rinsed twice in 0.1 M sodium cacodylate buffer and once in distilled water, then dehydrated using a graded ethanol series followed by propylene oxide and infiltrated overnight with Spurr's epoxy resin (Spurr Low Viscosity Embedding Kit; Sigma-Aldrich, EM0300-1KT). The eyes were then embedded in Spurr's resin and allowed to polymerize in a 70°C oven for 48 h. Tissue sections were obtained with an ultramicrotome (UltraCut-E; Reichert Technologies Life Sciences, NY, USA) using glass or diamond knives. Thin (70- to 80-nm thickness) sections were collected on copper 75/300 mesh grids and stained with 2% (v/v) uranyl acetate and Reynolds' lead citrate. Sections were viewed and micrographs obtained with a JEOL Model 100CX electron microscope (JEOL, USA; Peabody, MA, USA) at an accelerating voltage of 60 keV

Electroretinography (ERG)

Scotopic (dark-adapted) electroretinograms were recorded from control C57BL/6J and *Dhdds*$^{flx/flx}$ iCre^{+} mice after overnight dark adaptation. Animals were anesthetized by intraperitoneal injection of a ketamine-xylazine mixture, followed by pupil dilation with an ophthalmic Atropine solution. Flash stimuli were applied using a ColorDome system (DiagnoSys LLC, Lowell, MA, USA). The ERGs were recorded from both eyes simultaneously using DTL thread contact electrodes

(OcuScience®, Henderson, NV, USA), contacting the corneal surface with a conductive medium (Goniovisc® (hydroxypropylmethylcellulose 2.5%), Hub Pharmaceuticals, 17238061015-EA). A bite bar and a platinum electrode under the skin served as reference and ground leads, respectively. Scotopic responses were obtained in 16 increasing flash intensity steps (10^{-3} to 500 cd-sec/m^2). Individual scotopic a-wave and b-wave responses for each strain examined were averaged (n=7-12). Individual b:a wave ratios were calculated at all flash intensities ≥1.25 cd-sec/m^2, and group averages and standard errors were calculated (n=7-12). Following rod desensitization achieved by maintaining a constant background illumination, photopic (light-adapted) ERG responses were elicited with green light (520 nm) flicker illumination at 30 Hz, using an 8-step custom protocol with increasing flash intensities (10^{-1} to 30 cd-sec/m^2). Statistical analysis using one-way ANOVA and Student's *t*-test were performed on data acquired at individual flash intensities, using GraphPad® software.

TUNEL assay

To visualize cell death, the *in situ* fluorescence-based Terminal deoxynucleotidyl transferase dUTP nick end labeling (TUNEL) assay (for detection of apoptotic cell death) was utilized as described previously (Tu et al., 2013). Paraffin sections of control and *Dhdds*$^{flx/flx}$ iCre^{+} eyes were deparaffinized, and citrate buffer antigen retrieval was performed. Sections were subjected to TUNEL assay, using a DeadEnd™ Fluorometric TUNEL System (G3250; Promega Corporation, Madison, WI, USA), per the manufacturer's instructions. Permeabilized sections were treated with equilibration buffer (provided by manufacturer), followed by Terminal Deoxynucleotidyl Transferase (TdT) labeling for one hour at 37^0C. Labeling reaction was halted by incubating in SSC Stop Buffer (provided by manufacturer) for 15 min. Sections were quickly rinsed three times in PBS and immunohistochemistry using Iba-1 monoclonal antibodies (Abcam, Cat. #ab178846; 1:100, RRID: AB_2636859) was performed as described above. Sections were DAPI stained, and

mounted using Vectashield® mounting medium (Vector Laboratories). Confocal fluorescence micrograph images were captured using the 488 nm wavelength channel to detect TUNEL-positive cells.

PNGase-F assay

Retinas from PN 5-week-old wild type and *Dhdds*$^{flx/flx}$ iCre^{+} retina were isolated and lysed in SDS-free homogenization buffer (SDS interferes with PNGase-F activity). After protein quantification using BCA assay (see Western blot section, above), 50 µg of protein was subjected to non-denaturing PNGase-F assay (New England Biolabs Inc., P0704S) as per manufacturer's instructions. Briefly, the protein sample (50 µg) was treated with 2,500 U of PNG-ase F in 1X Glycobuffer (10X buffer provided with the kit) supplemented with 1% NP-40 detergent at 37^{O}C, overnight. PNGase-F-treated WT and *Dhdds*$^{flx/flx}$ iCre^{+} retinal protein extract were compared with untreated extract by Western blot analysis, probing the blots with anti-RHO antibody (see pertinent section above)

Cytokine Array

An unbiased, broad screening approach was utilized to test the upregulation of cytokines in the observed retinal degeneration. For this purpose, a membrane-based sandwich assay [Proteome Profiler Mouse Cytokine Array Kit, R&D Systems, Minneapolis, MN, USE; ARY006] was adapted as per manufacturer's instructions.PN 5 week old *Dhdds*$^{flx/flx}$ iCre^{+} and *Dhdds*$^{flx/flx}$ iCre^{-} retinal protein extract (n=3/group; 200 µg of protein extract/array) were mixed with a cocktail of biotinylated detection antibodies (kit content), and subsequently incubated with the mouse cytokine array membrane. The membrane was washed, and incubated with streptavidin-horseradish peroxidase for 1 h. Femto Chemiluminescence detection system (ThermoFisher,

34094) was used for signal amplification, and array imaging/signal detection was carried out on a BioRad ChemiDoc™ MP Imaging System. Background noise was subtracted from the cytokine-specific signal utilizing ImageLab software, and background-corrected signal ratio between *Dhdds*$^{flx/flx}$ iCre^{+} and *Dhdds*$^{flx/flx}$ iCre^{-} was calculated for individual cytokines.

Analysis of dolichol content

Five retinas were pooled and subjected to alkaline hydrolysis at 95°C for 1 h in hydrolytic solution (25% (w/v) KOH in 65% (v/v) ethanol, *aq.*). Nonsaponifiable lipids were then extracted three times with hexane, pooled extracts were evaporated to dryness under a stream of nitrogen, and the residue was dissolved in 2-propanol. UHPLC-ESI-HR-MS analyses of polyisoprenoids were performed by the method described in detail previously (Jozwiak et al., 2017), using an ACQUITY I-Class Ultra-Performance Liquid Chromatograph (Waters Corporation, Milford, MA, USA) coupled with a Synapt G2-S HDMS mass spectrometer (Waters) equipped with an electrospray ion source and quadrupole time-of-flight (q-TOF) mass analyzer. The chromatographic separation of polyisoprenoids was carried out using an Acquity BEH C18 column (2.1 x 100 mm, 1.7 µm) (Waters). Mass spectra of polyisoprenoid alcohols were recorded in the positive ion mode with the resolving power of a TOF analyzer 20000 FWHM. The exact mass measurements for all peaks were performed within 3 mDa mass error. The instrument was controlled and recorded data were processed using a MassLynx V4.1 software package (Waters).

SUPPLEMENTAL REFERENCES

BUTLER, M. C. & SULLIVAN, J. M. 2018. Ultrahigh Resolution Mouse Optical Coherence Tomography to Aid Intraocular Injection in Retinal Gene Therapy Research. *J Vis Exp*.

EMOTO, K., YAMASHITA, S. & OKADA, Y. 2005. Mechanisms of heat-induced antigen retrieval: does pH or ionic strength of the solution play a role for refolding antigens? *J Histochem Cytochem,* 53**,** 1311-21.

FLIESLER, S. J., PEACHEY, N. S., RICHARDS, M. J., NAGEL, B. A. & VAUGHAN, D. K. 2004. Retinal degeneration in a rodent model of Smith-Lemli-Opitz syndrome: electrophysiologic, biochemical, and morphologic features. *Arch Ophthalmol,* 122**,** 1190-200.

JOZWIAK, A., LIPKO, A., KANIA, M., DANIKIEWICZ, W., SURMACZ, L., WITEK, A., WOJCIK, J., ZDANOWSKI, K., PACZKOWSKI, C., CHOJNACKI, T., POZNANSKI, J. & SWIEZEWSKA, E. 2017. Modeling of Dolichol Mass Spectra Isotopic Envelopes as a Tool to Monitor Isoprenoid Biosynthesis. *Plant Physiol,* 174**,** 857-874.

LI, S., CHEN, D., SAUVE, Y., MCCANDLESS, J., CHEN, Y. J. & CHEN, C. K. 2005. Rhodopsin-iCre transgenic mouse line for Cre-mediated rod-specific gene targeting. *Genesis,* 41**,** 73-80.

MALUMBRES, M., MANGUES, R., FERRER, N., LU, S. & PELLICER, A. 1997. Isolation of high molecular weight DNA for reliable genotyping of transgenic mice. *Biotechniques,* 22**,** 1114-9.

RAMACHANDRA RAO, S., PFEFFER, B. A., MAS GOMEZ, N., SKELTON, L. A., KEIKO, U., SPARROW, J. R., ROWSAM, A. M., MITCHELL, C. H. & FLIESLER, S. J. 2018. Compromised phagosome maturation underlies RPE pathology in cell culture and whole animal models of Smith-Lemli-Opitz Syndrome. *Autophagy***,** 1-22.

TU, C., LI, J., JIANG, X., SHEFLIN, L. G., PFEFFER, B. A., BEHRINGER, M., FLIESLER, S. J. & QU, J. 2013. Ion-current-based proteomic profiling of the retina in a rat model of Smith-Lemli-Opitz syndrome. *Mol Cell Proteomics,* 12**,** 3583-98.

SUPPLEMENTAL FIGURES

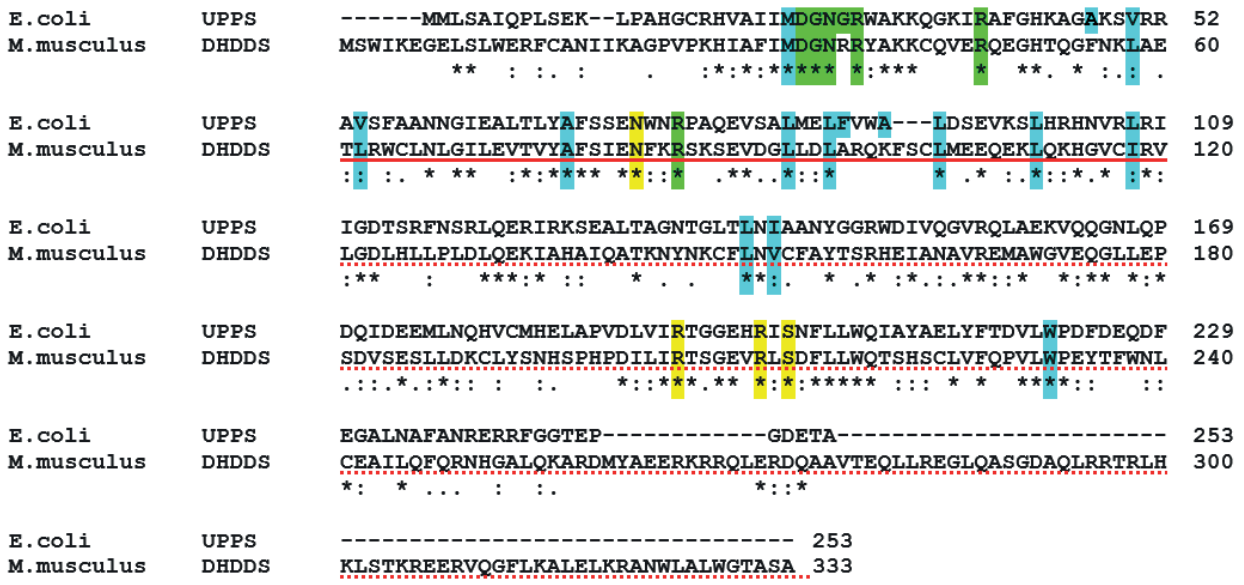

Figure S1. Multiple sequence alignment and comparison of FPP and IPP binding sites in the DHDDS complex. Related to Figure 1.

DHDDS is required for FPP and IPP condensation to generate polyprenol. Sequence alignment of murine (*M. musculus*) Dhdds against *E. coli* UPPS suggests conservation of critical amino acids required for FPP and IPP binding (*yellow, green highlights*), and hydrophobic interactions (*cyan highlights*). The conserved region required for FPP/IPP bindng is lost upon Cre-mediated excision of exon 3 of *Dhdds* (*solid red underline* corresponds to the region coded by exon 3; *dashed red underline* represents the peptide coded by downstream exons, which may not be translated due to the frameshift generated by deletion of exon 3). Notations: fully conserved (*); mostly conserved (**:**); partially conserved (**.**).

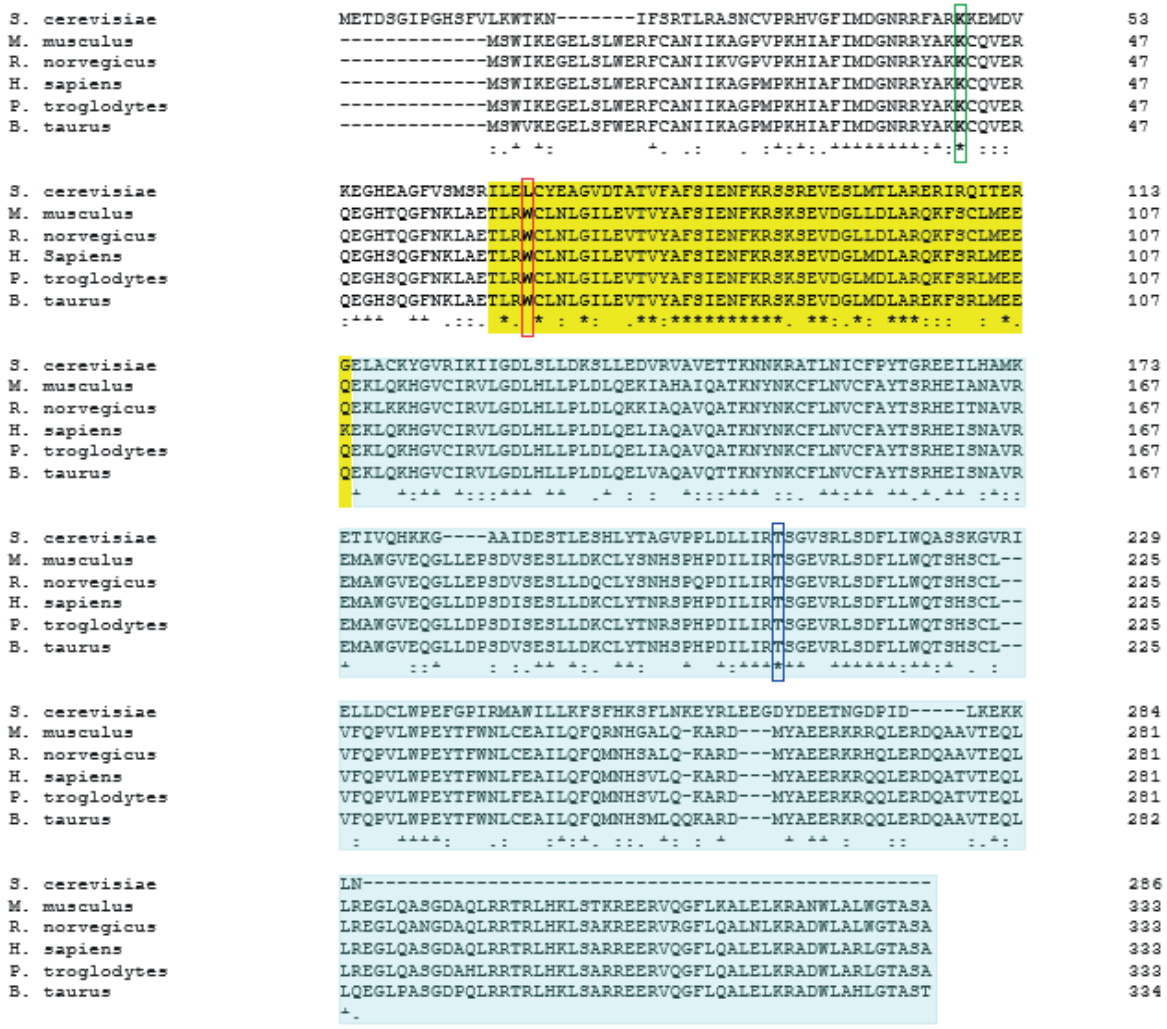

Figure S2. Multiple sequence alignment reveals species conservation of DHDDS FPP/IPP binding sites at the protein level. Related to Figure 1.

The peptide region coded by murine exon 3 of *Dhdds* (the targeted exon in this study, highlighted in *yellow*) is required for FPP binding, and is very well conserved between species. Critical FPP and IPP binding sites coded by exon 3 and downstream exons are highly conserved (see **Figure S1**). Known RP-associated DHDDS point mutations (K42E [*green box*], W64X [*red box*], T204A [*blue box*]) are shown. Downstream exons, which may not be translated due to the frameshift generated by deletion of exon 3, have been highlighted in cyan. Notations: fully conserved (*); mostly conserved (**:**); partially conserved (**.**).

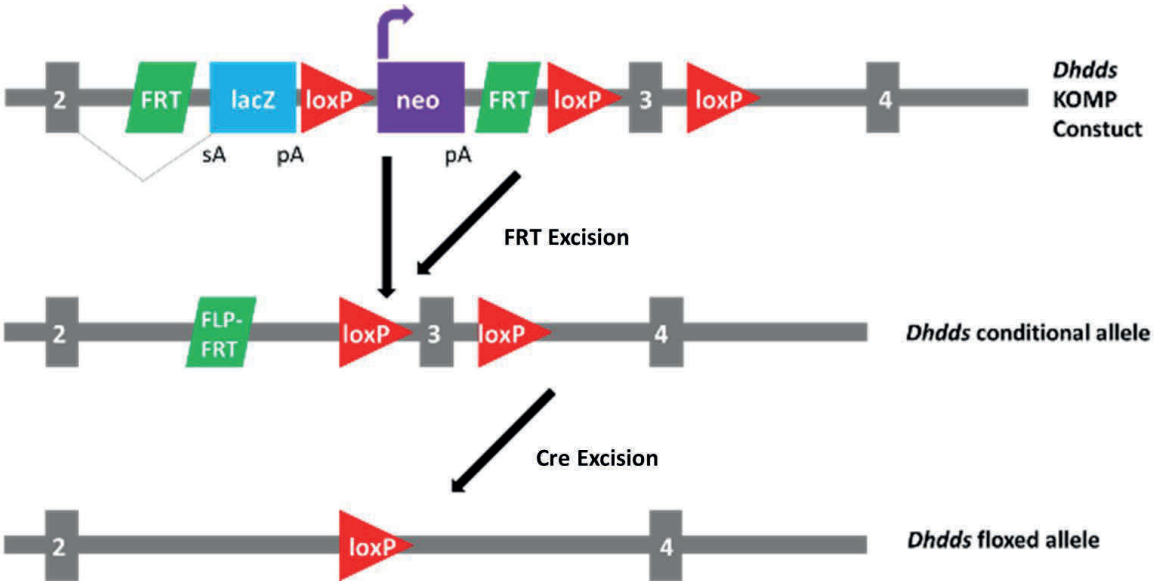

Figure S3. Knockout Mouse Project (KOMP) DHDDS conditional knockout alleles. Related to Figure 2.

A validated *Dhdds* plasmid construct was obtained from KOMP (U.C. Davis; Davis, CA, USA). The plasmid was linearized and introduced into mouse C57BL/6J mouse ES cells. Transformed cells were treated with FLP recombinase to excise the lacZ cassette, leaving a single FRT site. Confirmed FRT-excised ES cells were used to generate *Dhdds*$^{flx/flx}$ mice containing two loxP sites surrounding exon 3. Expression of Cre recombinase leads to excision of all sequence between the two loxP sites including all of exon 3, leaving behind a single loxP site.

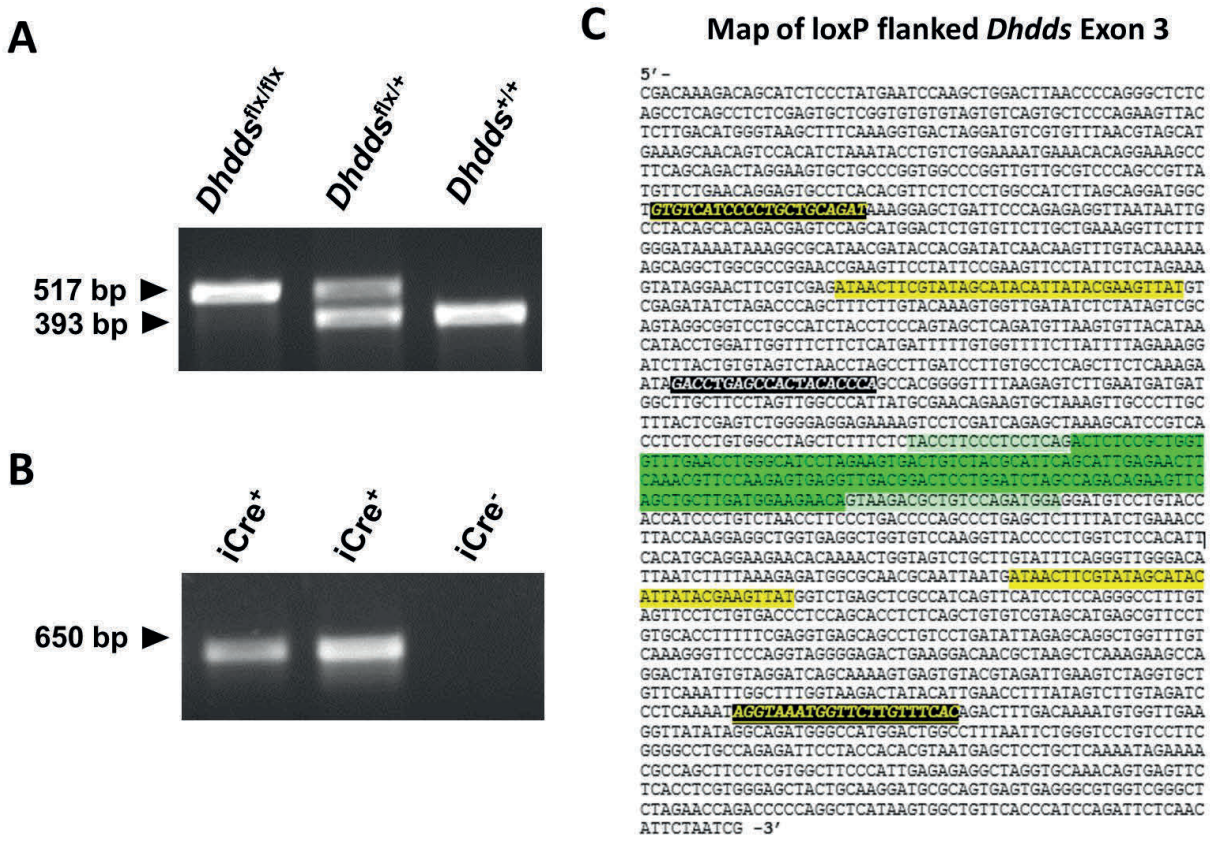

Fig. S4. Representative agarose gel image of initial PCR genotyping analysis using tail snip. Related to Figure 1.

A. Genomic DNA extracted from tail snips of *Dhdds*$^{flx/flx}$ iCre^{+}, *Dhdds*$^{flx/+}$ iCre^{+}, and *Dhdds*$^{+/+}$ iCre^{-} mice was subjected to PCR genotyping to differentiate the floxed *vs*. wild type alleles, as well as Cre recombinase status. The *Dhdds* WT allele yields a 393 bp product, while the *Dhdds* floxed allele yields a 517 bp product. **B.** PCR genotyping for the Rho- iCre allele. The Rho-iCre transgene yields a 650 bp product. **C.** The gene sequence of the loxP-modified *Dhdds* allele is shown, along with the PCR genotyping strategy and primer choices for tail snip and retinal genotyping (see **Figure 1**). The intronic region is highlighted in *cyan*, *Dhdds e*xon 3 is highlighted in *green*, upstream and downstream loxP sites are highlighted in *yellow*. Forward and reverse primers used in retinal genotyping are shown (*yellow text, black highlight*). Tail snip genotyping utilized the same forward primer as used for retinal genotyping; reverse primer for tail snip genotyping is shown (*white text, black highlight*).

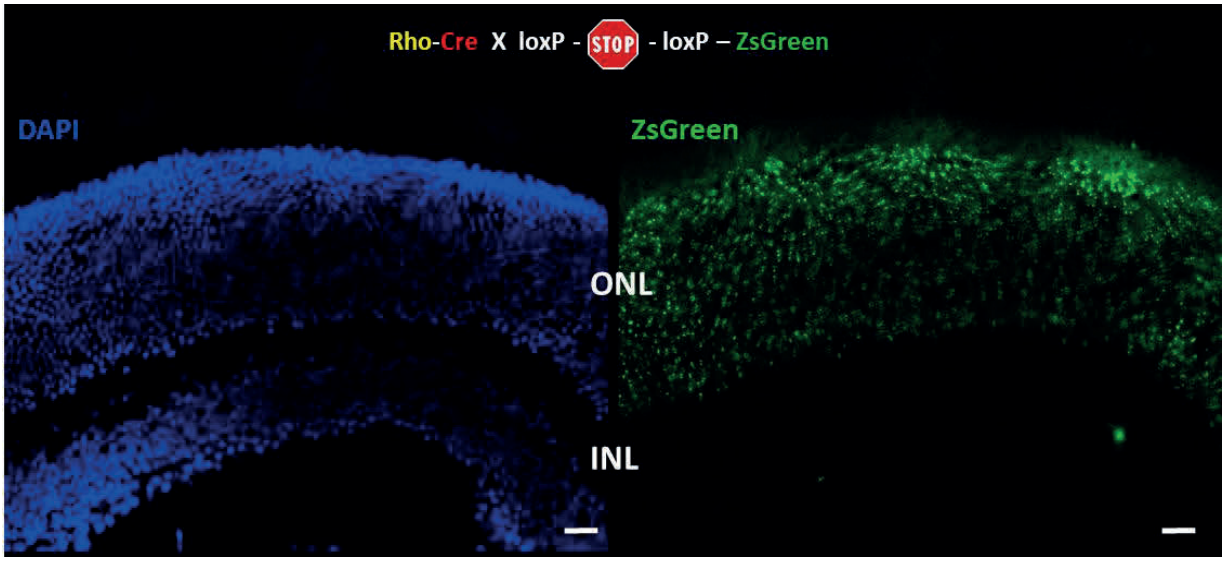

Figure S5. Cre recombinase activity is present in the majority of rod photoreceptors by PN 15 days. Related to Figure 2.

ZSgreen expression is exclusively expressed in rods, suggesting Rho-iCre activity. DAPI and GFP channels are shown separately to demonstrate ZsGreen expression exclusively in the majority of cells in the photoreceptor layer (~97% of which are rods) at PN 15 days. (See **Figure 2** for ZsGreen expression at PN 30 days.) [Scale bar: 20 μm.]

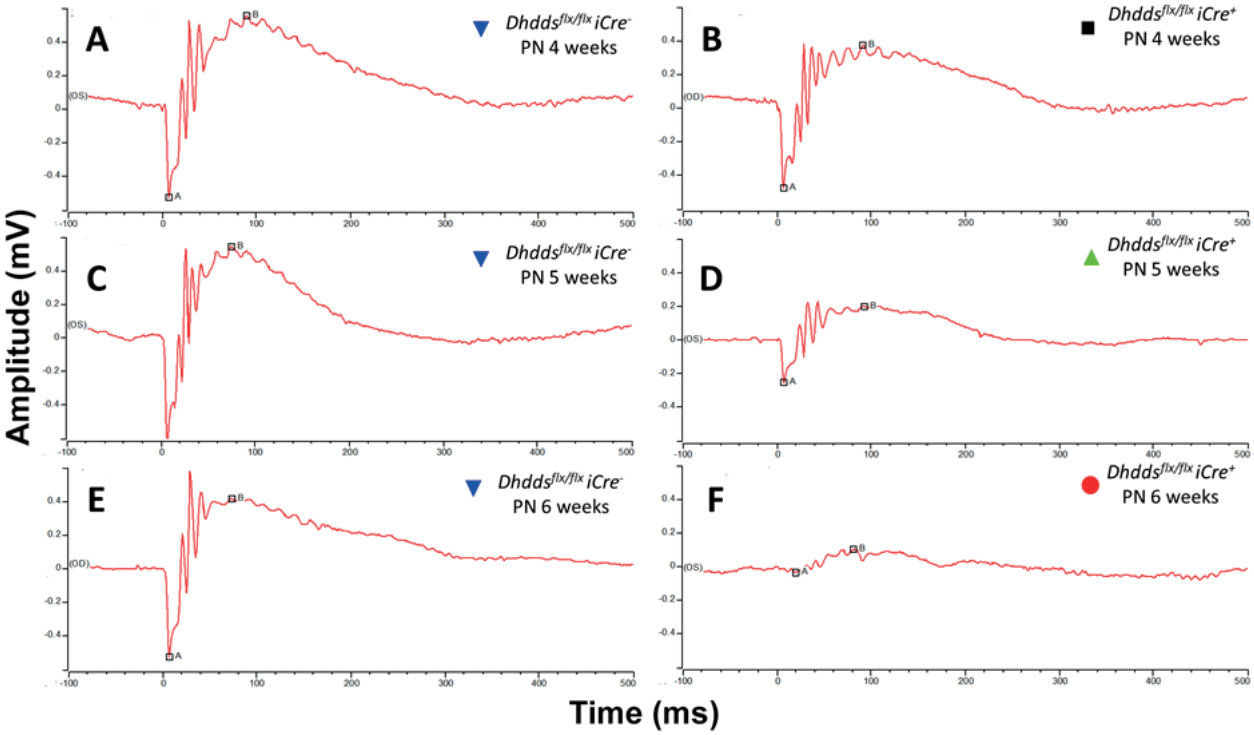

Figure S6. Representative scotopic ERG traces of age-matched *Dhdds*$^{flx/flx}$ iCre^{-} and *Dhdds*$^{flx/flx}$ iCre^{+} mice. Related to Figure 3.

Representative ERG traces of *Dhdds*$^{flx/flx}$ iCre^{+} mice (**B,D,F**) at highest flash intensity (500 cd-s/m^2) suggests rapid, age-related decline in scotopic response, compared to *Dhdds*$^{flx/flx}$ iCre^{-} mice (**A,C,E**), as observed in **Figure 3**. Scotopic ERG response in *Dhdds*$^{flx/flx}$ iCre^{+} mice were essentially extinguished by PN 6 weeks.

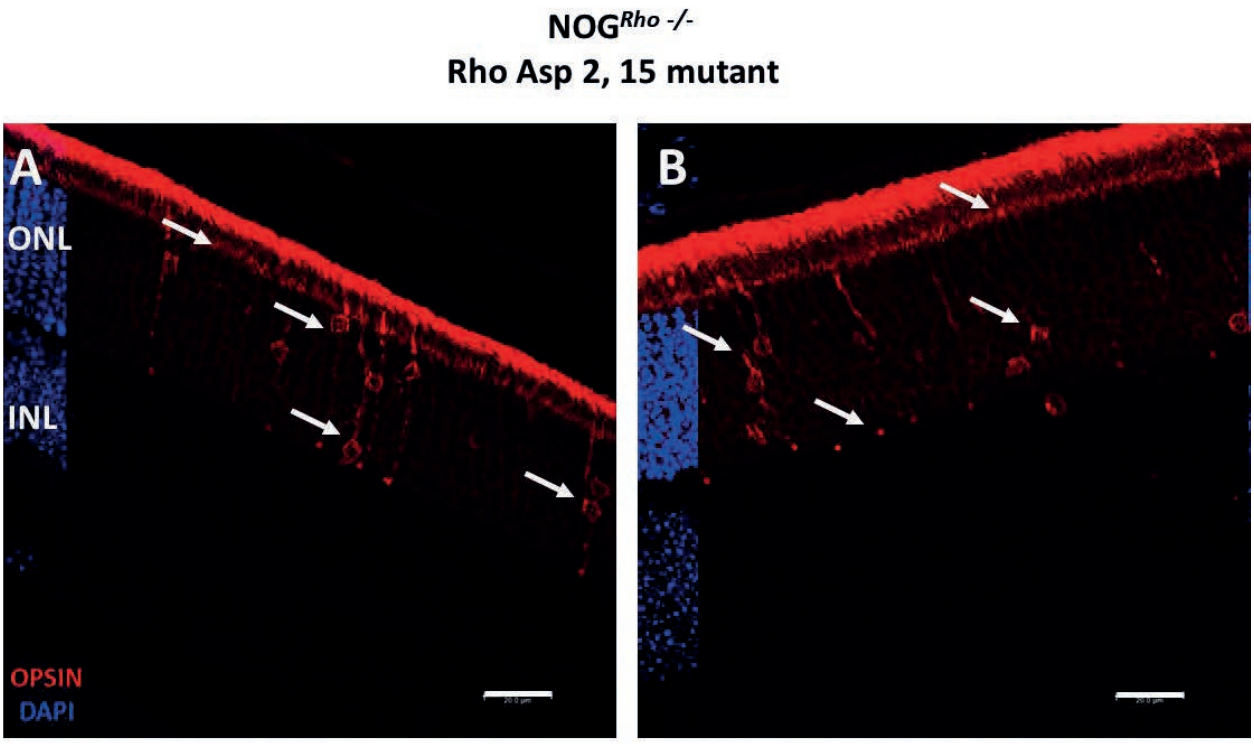

Figure S7. Demonstration of opsin trafficking defect in an established hypoglycosylation model. Related to Figure 5.
Immunohistochemistry using anti-opsin antibody to localize rhodopsin in the Nog$^{Rho-/-}$ mouse retina (a positive control for opsin hypoglycosylation) demonstrates defective intracellular trafficking of opsin. Opsin mislocalization leads to IS (*arrows*) and perinuclear (*arrowheads*) accumulation. DAPI staining (*blue*) is shown on the left-hand side of each micrograph. This is in agreement with the lack of obvious *N*-glycosylation defects observed in **Figure 5.** [Scale bar: 20 μm.]

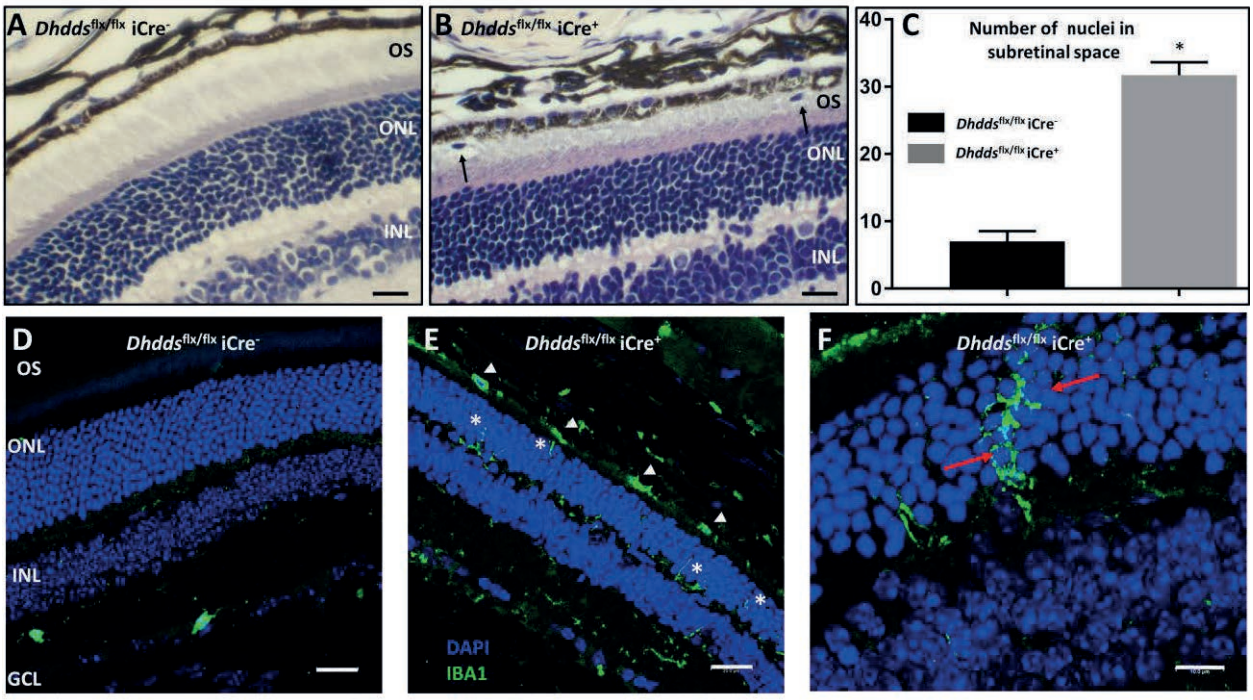

Figure S8. *Dhdds*$^{flx/flx}$ iCre^{+} retina exhibits significant increase in cells in the subretinal space. Related to Figure 4.

Further characterization of microglial infiltration and phagoptosis. **(A, B)** Histology of control and *Dhdds*$^{flx/flx}$ iCre^{+} retinas, respectively, at PN 5 weeks of age (H&E staining). Quantification of cells in the subretinal space was performed on retinal tissue sections of each genotype (8 eyes per genotype, 3 sections per eye; 10-µm thickness). This compartment of the retina normally is occupied by photoreceptor outer segments and extracellular matrix, but not other cells. However, H&E-stained cells were present in this retinal layer in *Dhdds*$^{flx/flx}$ iCre^{+} mice (**B**, *black arrows*). The same region shown in a control retina (**A,** *open bracket*) is devoid of mislocalized cells, although the far peripheral regions of control retinas were observed to contain such cells (*not shown*). (**C**) Quantitative analysis of mislocalized cells as a function of genotype; a 4-fold increase was observed in the number of such cells in *Dhdds*$^{flx/flx}$ iCre^{+} retinas, relative to controls. (**D-F**) In the young, control mouse retina, horizontally ramified, Iba-1-positive microglia were observed only in the inner retinal layers (**D**). By contrast, the *Dhdds*$^{flx/flx}$ iCre^{+} mouse retina shows microglial infiltration into the ONL (**E,** *asterisks*), as well as in the subretinal space and outer segment (OS) layer (**E,** *arrowheads*). A representative higher magnification image of a *Dhdds*$^{flx/flx}$ iCre^{+} mouse retina shows activated, Iba-1-positive microglia surrounding photoreceptor nuclei, indicative of active “phagoptosis” of live photoreceptors by microglia (**F,** *red arrows*). [Scale bars: **D**, **E,** 20 µm; **F,** 10 µm.]

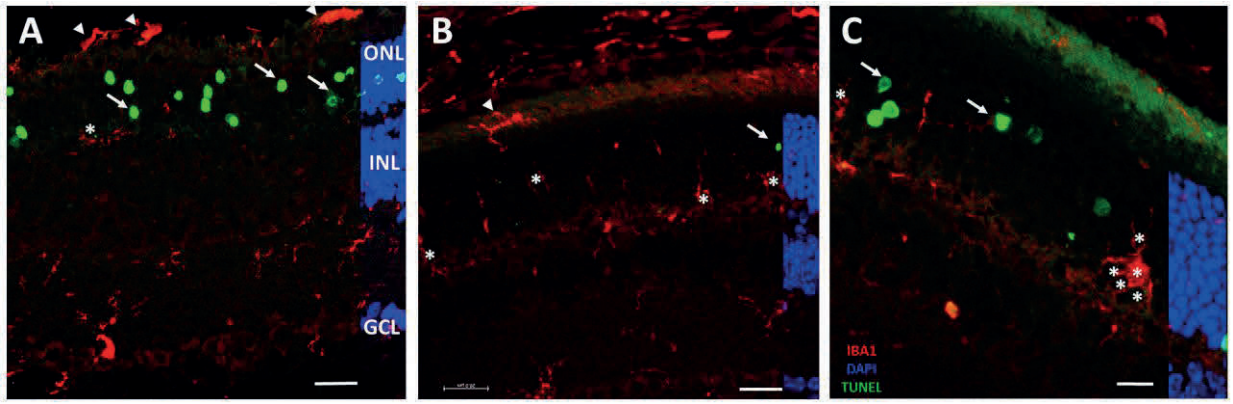

Figure S9. Cell-autonomous photoreceptor cell death and phagoptosis in *Dhdds*$^{flx/flx}$ iCre^{+} mice. Related to Figure 4.

Additional representative confocal micrographs (**A-C**) demonstrate TUNEL-positive photoreceptor cells (*white arrows*, green channel), as well as phagocytic uptake of live, TUNEL-negative photoreceptors by Iba-1-positive microglial cells (*asterisk*, red channel). Iba-1-positive microglial cells were found in the subretinal space (*white arrow head,* red channel). DAPI labeling of the nuclear layers is shown on the right-hand side of each image. [Scale bars: (**A, B**) 20 μm; (**C**) 10 μm.]

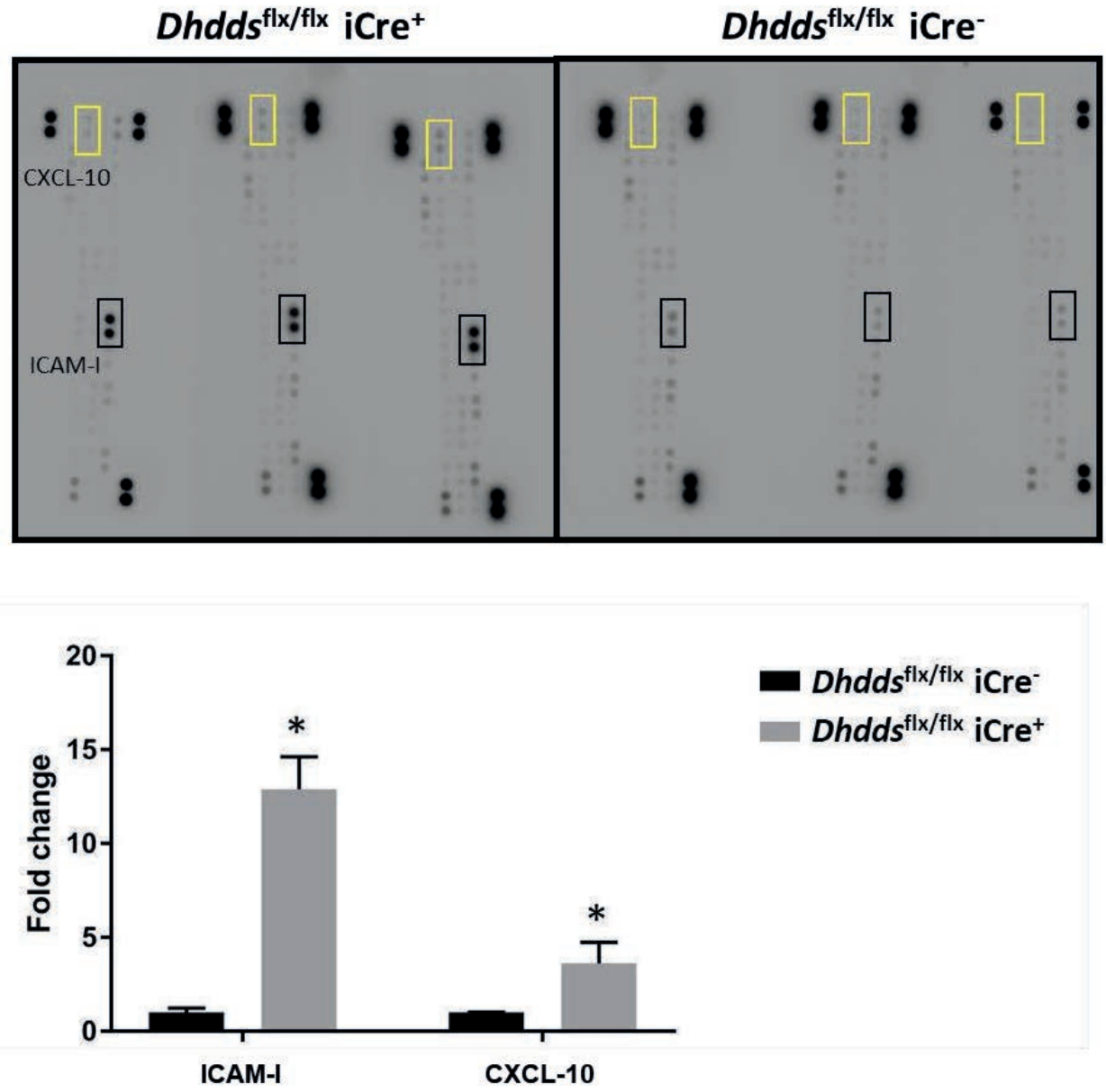

Figure S10. Sandwich ELISA-based cytokine array analysis of retinal extracts from PN 5-week old *Dhdds*$^{flx/flx}$ iCre^{+} and control mice. Related to Figure 4.
Representative ELISA assay results for the presence of selected cytokines (CXCL-10 and ICAM-1). Background-subtracted luminescence signal was measured using ImageLab® software. Significant increases in retinal ICAM-1 and CXCL-10 levels (*$p<0.01$, n=5/group) were observed in *Dhdds*$^{flx/flx}$ iCre^{+} mice, compared to controls. This is further characterization of ICAM1 upregulation as observed by Western blot analysis (see **Figure 4**).

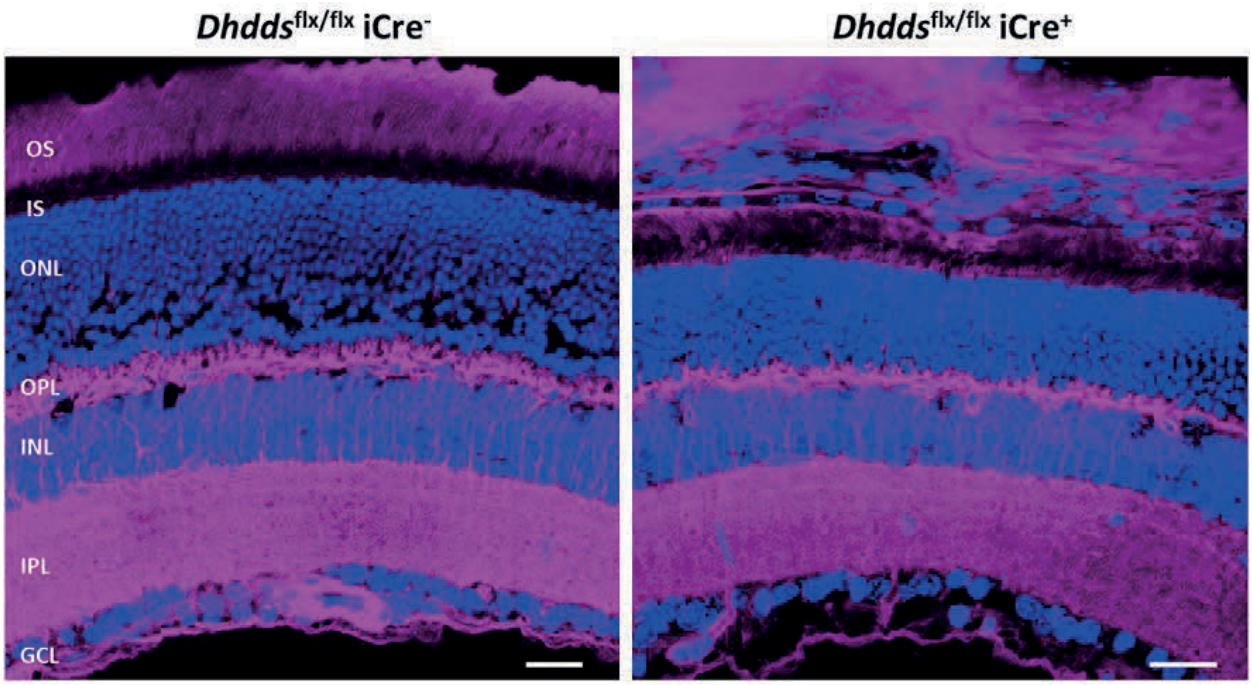

Fig. S11. Lectin cytochemistry demonstrates fluor-conjugated wheat germ agglutinin (WGA) binding to retinal photoreceptors in *Dhdds*$^{flx/flx}$ iCre^{+} mice. Related to Figure 5.
WGA (pseudocolored *magenta*) selectively binds to β-1,4-GlcNAc-containing extracellular matrix components surrounding rod, but not cone, photoreceptors as well as the extracellular matrix in the ONL. Note the comparable, robust WGA staining of retinas from PN 5-week old *Dhdds*$^{flx/flx}$ iCre^{+} (*right panel*) and control (*left panel*) mice. This is in agreement with the lack of glycosylation as observed in **Figure 5.** [Scale bar: 20 μm.]

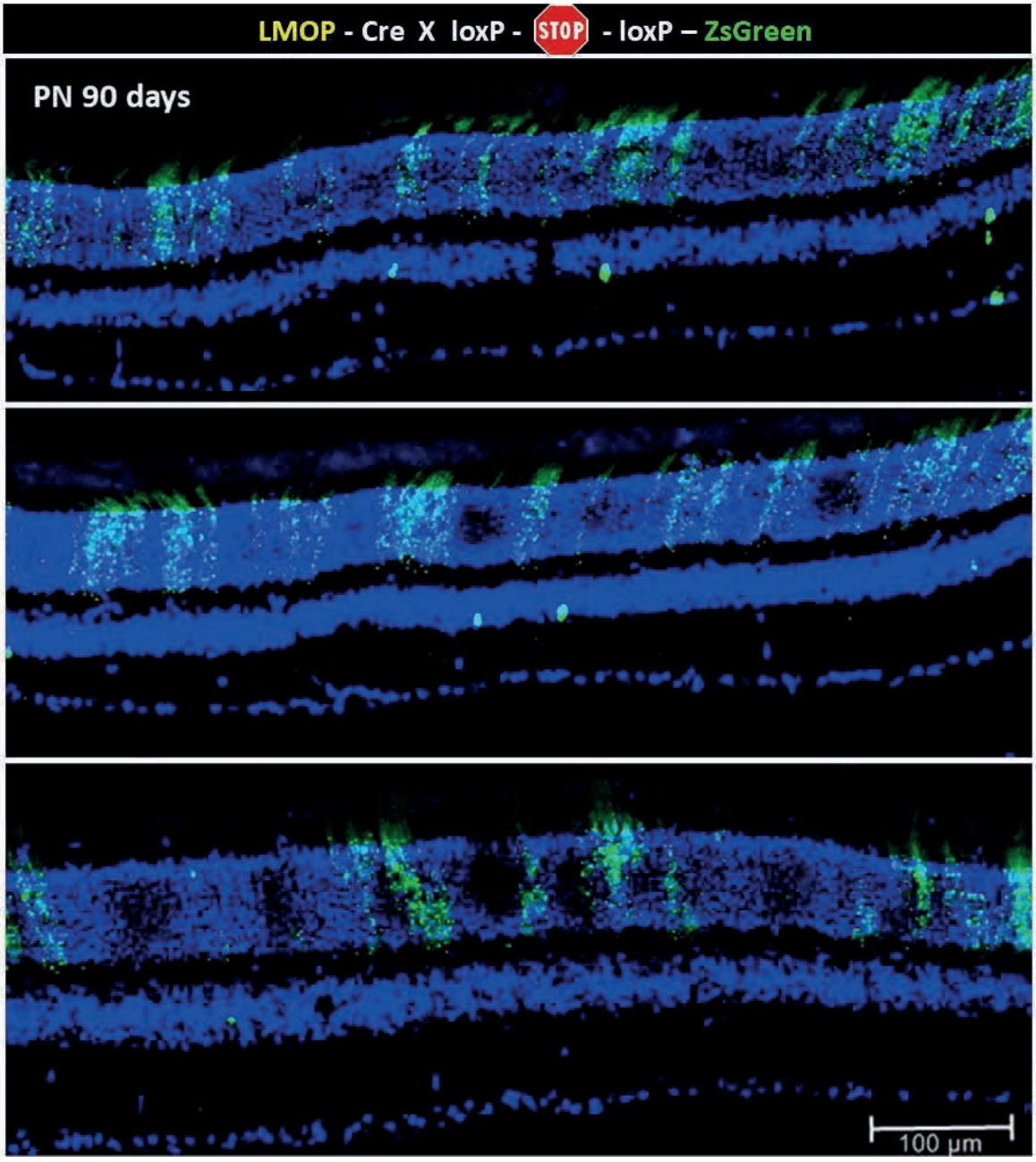

Figure S12. Mozaicism of Cre recombinase activity in the LMOP Cre mouse line. Related to Figure 2.
LMOP-Cre mice were crossed with ZsGreen reporter mice. Representative confocal microscopy images of mouse retinas (n=3, PN 3-month old) exhibit patchy expression of ZsGreen, which is inconsistent with the expected uniform distribution of rhodopsin in that layer of the mouse retina. [Scale bar: 100 µm.] Hence, for this study, we chose instead to utilize the Rho-iCre75 mouse line for generation of the rod-specific *Dhdds* knockout mouse line (*Dhdds*$^{flx/flx}$ iCre^{+}) described herein.

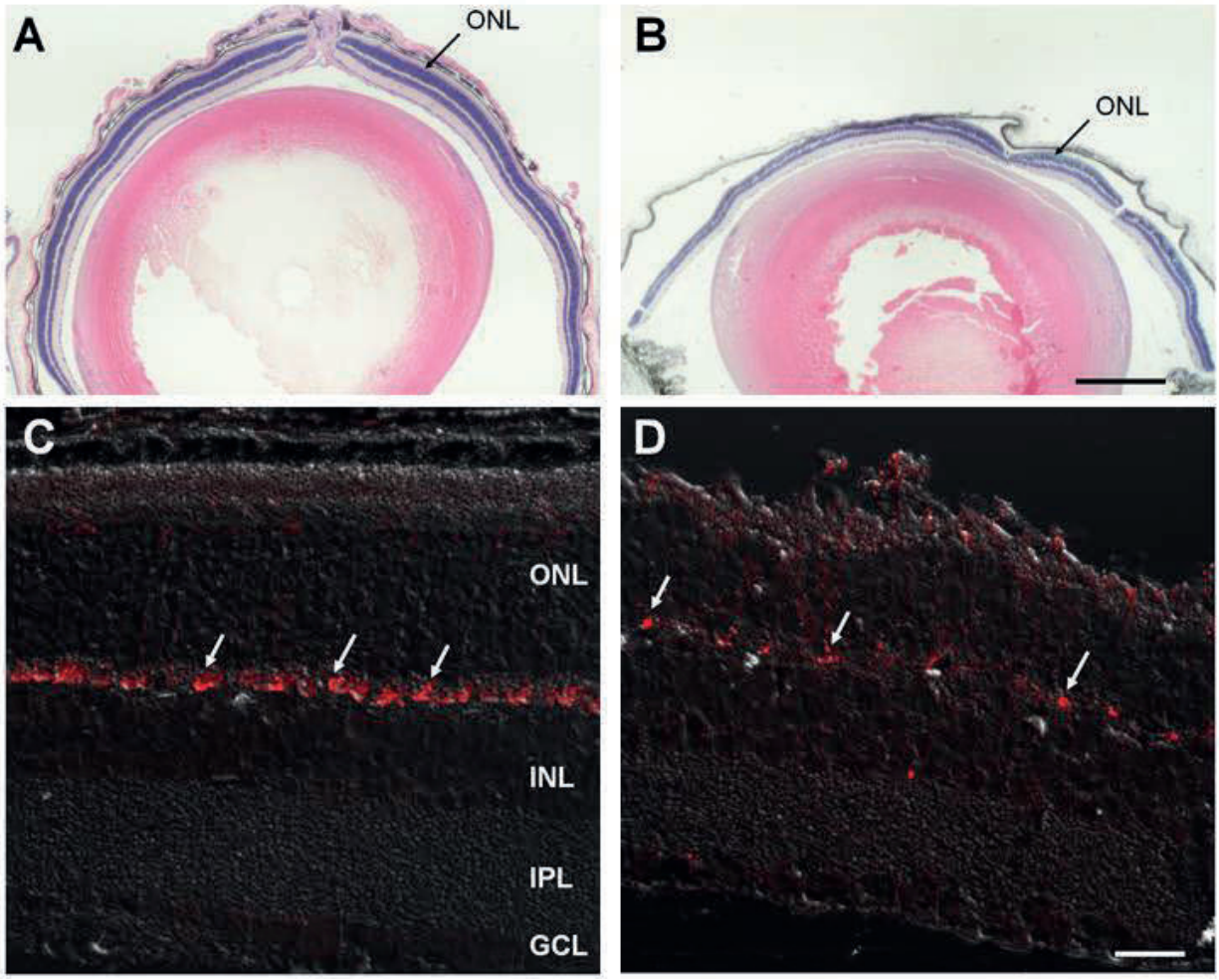

Figure S13. Low magnification image depicting retinal thinning and persistence of cone photoreceptors. Related to Figures 2 and 3.

Spectral domain optical coherence tomography (SD-OCT) imaging demonstrated significant thinning of the *Dhdds*$^{flx/flx}$ iCre^{+} retina (see **Figure 2**). Low-magnification light micrographs of H&E-stained control (**A**) and PN 5- week old *Dhdds*$^{flx/flx}$ iCre^{+} mice (**B**) also demonstrate significant thinning of the photoreceptor layer in *Dhdds*$^{flx/flx}$ iCre^{+} mice. Immunohistochemical analysis of ocular tissue sections from control (**C**) and *Dhdds*$^{flx/flx}$ iCre^{+} (**D**) mice, stained with anti- cone arrestin antibody (pseudocolor: *red*), demonstrating arrestin-positive cone synaptic termini as well as immunopositive elements in the inner and outer segment layer regions. [Scale bar: (**A,B**) 500 µm; (**C,D**) 20 µm.